ORIGINAL ARTICLE

Jackfruit peel derived ZnCl$_2$-impregnated activated carbon: Optimization, characterization, and application in dye removal

Pratima Minz[1] · Susmita Mishra[1]

Abstract

The research has aimed to demonstrate an optimization methodology to reliably obtain carbon by chemical activation method using Jackfruit peel powder (JPP) as the primal matter. Response surface methodology (RSM) assessed and optimized the synthesis process parameters. The studied input parameters were carbonization temperature, activation time, and impregnation ratio (ZnCl$_2$:JPP), and the iodine adsorption value and yield percentage of the prepared activated carbon were the analyzed responses. Box-Behnken design approach was utilized to prepare models based on quadratic regression equations. The results proclaimed that activated carbon of yield 46.16% and iodine adsorption value of 1090.44 mg/g can be obtained at 89 min of activation time and an impregnation ratio of 0.74. The characterization of optimized activated carbon was done by SEM-EDX, FTIR, and XRD, followed by wielding as an adsorbent, which resulted in 97% removal of Remazol golden yellow, an anionic dye from the aqueous solution. Freundlich isotherm model and pseudo-second-order model represented the experimental data better. The synthesized carbon exhibited the potential to be utilized at least 5 times with higher removal efficiency.

Keywords Jackfruit peel · ZnCl$_2$ · Activated carbon · RSM-BBD · Optimization · Dye removal

1 Introduction

Agriculture is an absolute necessity for living being. Globally, the agriculture sector produces 24 million tons of food annually [1]. In the present scenario, to meet the high demand of a fast-growing population, abundant agricultural waste is being generated. Among them, India produces approximately 350–990 Mt of agricultural waste (biomass) every year, which includes industry wastes (peels, pulps, bagasse, etc.), crop residues (stems, leaves, husks, etc.), and live stocks, etc. Biomass consists of one of the vital and major constituents, i.e., lignocellulose (cellulose, hemicellulose, and lignin) [2]. Lignocellulosic biomass is versatile and has been extensively explored for the synthesis of several value-added products, namely compost, bio-bricks, concrete, bioethanol, biogas, biochar, and activated carbon, etc., which can be of commercial importance. Additionally,

valorizing biomass could simultaneously reduce the existing waste management crisis.

Activated carbon (AC) is a highly porous structured substance, an efficient adsorbent for gas and water applications. AC has also been used as catalyst support, gas storage, supercapacitors, etc. The global AC market is estimated to be 6 billion USD in 2023 [3], and it is projected to reach 7.5–9 billion USD by 2030, with an apparent increment in production of 10% every year [4], which indicates the rising demand. Commercially produced AC contains a marvelous porous matrix undoubtedly. However, it carries economic limitations of high material and regeneration costs, which mandates a substitute precursor (i.e., ubiquitous, affordable, and renewable) [5]. In this regard, lignocellulosic biomass waste is an inevitable replacement as the precursor, which is relatively less expensive, easily available, abundant in nature, and most effective for specific absorption-related applications, etc. A variety of lignocellulosic biomass wastes has been explored as precursors for AC preparation, such as coconut shell [6], bael fruit [7], barley husk [8], date stones [9], date palm bark [10], Limonia acidissima shell [11].

Preparation of AC consists of two major steps, including high-temperature carbonization in an inert atmosphere

✉ Susmita Mishra
smishra@nitrkl.ac.in

1 Department of Chemical Engineering, National Institute of Technology Rourkela, Odisha, India

and subsequent activation of the material. Carbonization leads to the development of pore structure which is rudimentary in nature. However, activation causes enhancement of pore diameter and results in nucleation of pores. Some of the exemplary work associated with chemical activation are mentioned as follows: Ozsin et al. [12] used KOH and K_2CO_3 as activating agents, and chickpea husk was the primal matter for the production of AC. Similarly, Genli et al. [13] employed hydrothermal carbonization for the chemical activation of the carbon using KOH. Several other works also reported H_3PO_4 [14], H_2SO_4 [15], $ZnCl_2$ [16], and NaOH [17], etc. as activating agents. Among these, $ZnCl_2$ is known for outstanding performance as an activator. Polymerization occurs by $ZnCl_2$ activation results in high yield, and Lewis acid nature creates ring-type aromatic compounds, leading to uniform pore formation [18]. In another work, Astuti et al. [19] observed that $ZnCl_2$ creates a template effect forming uniform pores in the pineapple leaf and coconut shell-based AC. Therefore, $ZnCl_2$ could be a potential candidate to improve the characteristics of carbon matrix derived from unexploited biomass precursors.
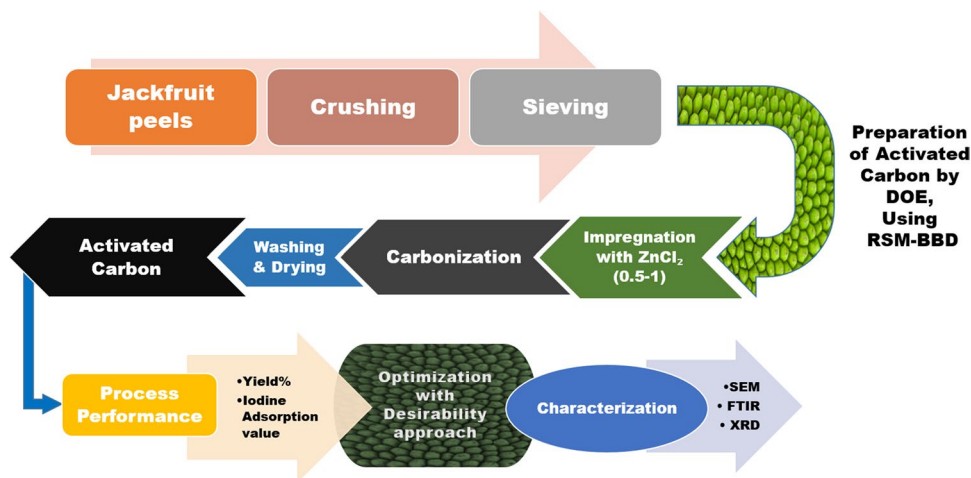
Jackfruit (*Artocarpus heterophyllus*) is one such source of biomass precursors that are harvested in many tropical Asian countries (Indonesia, Myanmar, Thailand, Vietnam, India, etc.). In India, approximately 26,000 hectares of land are utilized for jackfruit farming. Around 60% of the fruit is inedible (central core, reed, peel, and seeds) and is considered bio-waste. An enormous amount of 3000–12,000 kg of waste could be generated and discarded just from a single tree [20]. The disposal of such huge wastes can lead to environmental issues, including water pollution, greenhouse emission, and asphyxiation [21]. In this context, few works have been reported on the jackfruit peel-based AC using KOH and H_3PO_4 [22–24]. These AC materials have been used to remove Malachite green dye, develop supercapacitor devices, and remove ciprofloxacin,

respectively. However, $ZnCl_2$-based activation of jackfruit peel AC is yet to be explored.

In the last few decades, the application of agricultural waste-based AC for the removal of synthetic dyes (from industries of textiles, food, paper, and pharmaceuticals) has gained immense attention. Synthetic dyes are of toxic nature (carcinogenic and mutagenic) even at lower concentrations and pose a serious threat to human health. They are highly stable compounds exhibiting resistance against light, oxidizing agents, and aerobic digestion [18]. Recently, Behloul et al. [25] studied the removal of CI Reactive red 141 using waste cotton fiber $ZnCl_2$ treated carbon with a maximum removal of 98.61%. Similarly, Suhaimi et al. [5] treated crystal violet dye wastewater by employing AC prepared from a mixture of carrot juice pulp and pomegranate peel with an adsorption capacity of 211.8 mg/g. Another study by Quimada et al. [16] removed EBT dye by adsorbing onto $ZnCl_2$-impregnated residual ground coffee AC with the removal of 93.26% and 92.66% in batch and column studies, respectively. Therefore, it is evident that chemically treated agricultural waste-based AC has demonstrated great potential in dye-removal applications.

Thus, this study aims to synthesize carbon from jackfruit peel powder (JPP) which is chemically activated by zinc chloride ($ZnCl_2$) using a mathematical modeling technique (RSM-BBD). The experimental effects of the process parameters (impregnation ratio, activation time, carbonization temperature) were analyzed on the responses of yield percentage and iodine adsorption value. Along with proximate analysis and TGA, properties of the optimized AC were analyzed through SEM-EDX, FTIR, and XRD. Additionally, the efficiency of the optimized AC was investigated for the removal of an industrial dye (Remazol golden yellow) from an aqueous solution. The preparation methodology of activated carbon is represented in pictorial form in Fig. 1.

Fig. 1 Preparation methodology

2 Materials and methods

2.1 Materials

Jackfruit (*Artocarpus heterophyllus*) utilized for the preparation of precursor was garnered from NIT Rourkela campus. Prior to use, the whole jackfruit was washed and cut into miniatures. The pulp and peel were segregated, followed by rinsing in distilled water, causing the obliteration of foreign particles, and lastly, overnight dried in a hot air oven at 60°C and pulverized in a ball mill. Zinc chloride ($ZnCl_2$) powder from Merck was utilized as activating agent. The Remazol golden yellow was acquired from SRL Chemicals Ltd. Double distilled water was utilized for solution preparation.

2.2 Characterization of precursor material

The size of the particle was maintained to be at a uniform size below 1mm. Proximate analysis (ASTM D121), including moisture content, volatile matter, ash content, and fixed carbon, was performed to recognize the characteristics and elements of the bio-matter. Thermogravimetric analysis (TGA) was performed to determine the thermal behavior of the primal matter. It was checked from room temperature to 600°C at a 10°C/min rate in an inert atmosphere.

2.3 Activated carbon synthesis

In order to synthesize AC, specific amounts of precursor (JPP) combined with $ZnCl_2$ at different impregnation ratios were amalgamated and impregnated at 90°C followed by drying at 120°C. In the tubular furnace, the dried sample was pyrolyzed at certain parameters, and the carbon obtained was washed in double distilled water until it achieved a neutral pH value [11].

2.4 Statistical optimization

Response surface methodology (RSM) provides a statistical method for observing the interaction between more than one experimental parameter (process parameter), namely, impregnation ratio, activation time, and carbonization temperature, on the evaluated process response(s). The chemical activation was assessed by the function of two responses: yield of the activated carbon (Y_1) and the adsorption of the activated carbon in the form of iodine value (Y_2). The estimation of Y_2 is estimated as per standard procedure [ASTM D607].

Table 1 Design parameters and levels used for optimization in Box-Behnken design

Factors	Code	Low level (−1)	High level (+1)
IR	A	0.5	1
Activation time (min)	B	30	90
Carbonization temperature (°C)	C	400	700

2.5 Design of experiment and statistical analysis

Design of experiments (DOE) analyzes the interaction between the various process parameters and their effect on the responses in order to estimate the optimal parameter values. RSM is preferred since it reduces experimental runs, which reduces the amount of resources and time spent on testing. The Box-Behnken design (BBD) is a practical design for fitting a second-order response-surface model, which has been implemented for the experimentations. The software used for this optimization was version 13 of Design-Expert (Stat-Ease Minneapolis, USA). The number of experimental runs (N) was established by the equation as follows:

$$N = (K - 1)(2K) + C_0 \tag{1}$$

where K is the total number of process parameters, and C_0 is the total number of central points.

All the predictions of the multiple responses were based on a polynomial regression model equation of 2nd order, which is as follows:

$$N = \beta_0 + \sum_{i=1}^{k} \beta_i x_i + \sum_{i=1}^{k} \beta_{ii} x_i^2 + \sum_{i=1}^{k-1} \sum_{j=2}^{k} \beta_{ij} x_i x_j \tag{2}$$

where β represents the coefficient of regression which is in the response of x; β_0 is the constant term, β_i is presenting the effect of the linear terms, β_{ii} is presenting the effect of quadratic terms, β_{ij} is for the effect of the interaction of the parameters. x_i and x_j are certain process parameters. Analysis of variance (ANOVA) is used for statistical analysis, and it determines the interaction among the factors and responses based on the model proposed. The regression model's quality is determined by the extracted coefficient of determination (R^2, R^2_{adj}), the residue analysis, and the correspondence between the actual and the predicted values. The p value (probability value) decides whether the model will be selected or rejected with a 95% confidence level.

Current work represents RSM in the form of three factors and two levels BBD where the factors are impregnation ratio (IR) which is the ratio of $ZnCl_2$ and the carbon source,

activation time, and carbonization temperature. The effect of these 3 parameters, along with their interactive effects on iodine value and yield, is mentioned and analyzed. All the process parameters and their ranges are mentioned in Table 1. Calculation of the total number of experimental runs (N) was done for twelve factorial points and five midpoints, which is as per the equation mentioned earlier:

$$N = (k - 1) (2k) + C_0 = (3 - 1) (2 * 3) + 5 = 17 \quad (3)$$

The optimization of each of the parameters for multiple responses was carried out using the desirability function. Desirability for each of the responses (y_i) is set as per the priorities. It is denoted as d_i (individual desirability function), which ranges from 0 to 1. 0 represents non-desirability, and 1 represents fully desired. Within the range, it is in accordance with less or more desirable. Combining all the individual desirability functions, an overall desirability function (D) is extracted. The more the D value is closer to 1 more splendidly acceptable the estimate would be. In the current work of BBD, the desirability approach is applied to obtain the responses (yield and iodine value), which were maximized for the synthesis of carbon from JPP.

2.6 Characterization of precursor and activated carbon

The topographical characteristics of the raw precursor (JPP) sample, along with the optimized activated carbon, were investigated in SEM. The coating was performed with a thin layer of gold on the samples for the purpose of charge dissipation during the imaging. For the quantitative chemical composition of the activated carbon and the precursor, EDX was performed using JEOL JSM-6700F. Adsorption or surface reactions are dependent on various types of functional groups, and interpretation of the functional groups on the precursor and the activated carbon was made by Fourier Transform Infrared Spectroscopy (FTIR) spectra for a spectral region of 4000^{-1} to 400^{-1} cm^{-1}. The X-ray diffraction was performed in the Rigaku Ultima IV instrument, which was equipped with Cu Kα radiation (40KV, 40mA) with a wavelength of 1.78901 Å on a setup size of 0.02. The rate of the scan was 10° per 60 s with a 2θ value of range 10 to 80°.

2.7 Adsorption study

The activated carbon was examined for the removal of Remazol golden yellow (an anionic dye) from the aqueous solution. A stock solution of 500 mg/l of the adsorbate (RGY) was diluted to acquire different concentrations for the study. Multiple parameters were tested to obtain maximum percentage removal: pH of the working solution, contact period of adsorbent and the adsorbate, amount of adsorbent, and initial concentration of the adsorbate. The working solution was 50 ml. Adjustment of pH was done by 0.1M HCl and 0.1M of NaOH. The detection was done in UV spectrophotometer (Shimadzu UV-1800) at a wavelength of 420nm. The equation of percentage removal is

$$\%R = \frac{C_o - C_f}{C_o} * 100. \quad (4)$$

C_o is the initial concentration of the RGY in the aqueous solution, and C_f is the final concentration of the RGY.

2.7.1 Adsorption isotherm study

Isotherm equilibrium data investigates the properties of adsorbents, mainly the adsorption mechanism and maximum adsorption capacity [26, 27]. For equilibrium modeling for Remazol golden yellow adsorption, the Langmuir adsorption model and the Freundlich adsorption model were employed.

Langmuir represents monolayer adsorption which can be due to any of the chemical and physical interactions or both between the adsorbent and the active sites. It is presented by the following equation in linear form:

$$\frac{C_e}{q_e} = \frac{1}{q_m K_L} + \frac{C_e}{q_m} \quad (5)$$

where q_m is monolayer adsorption capacity (mg/g), K_L is Langmuir adsorption constant (L/mg), and C_e is the equilibrium concentration.

Freundlich represents multilayer adsorption, and the linear equation goes as follows:

$$\ln q_e = \ln K_F + \frac{1}{n} \ln C_e \quad (6)$$

where K_F is Freundlich constant ($(mg/g)(L/mg)^{1/n}$), and n is the empirical parameter implying the adsorption intensity.

2.7.2 Kinetic study

Pseudo-first-order and pseudo-second-order models were used to investigate the adsorption mechanism and acquire kinetic parameters. The linear form of pseudo first order and second order is presented as follows, respectively.

$$\log (q_e - q_t) = \log q_e - \frac{K_1 t}{2.303} \quad (7)$$

$$\frac{t}{q_t} = \frac{1}{K_2 q_e^{2}} + \frac{1}{q_e} t \quad (8)$$
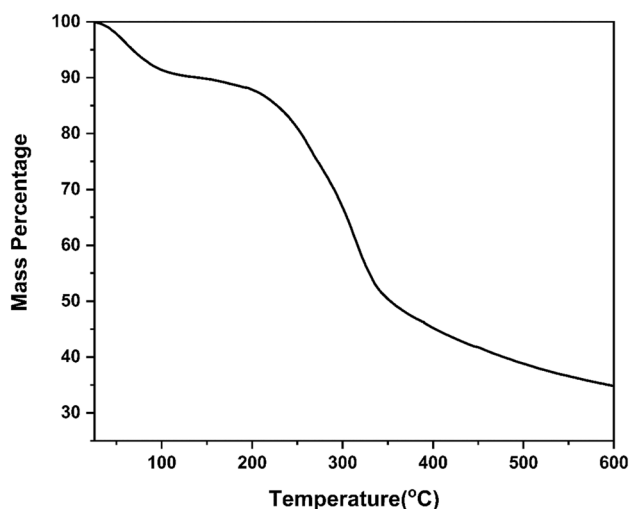
Fig. 2 Thermogravimetric analysis of JPP

Table 2 Experimental design matrix for yield% and iodine no. of ZnCl$_2$-AC

Run	Factor-1 A: IR	Factor-2 B: Time min	Factor-3 C: Temp °C	Response-1 Yield %	Response-2 Iodine no. mg/g
1	0.75	60	550	52.74	963.663
2	1	90	550	50.82	1001.5
3	0.75	60	550	51.08	978
4	0.5	30	550	50.32	846.63
5	1	30	550	66.3	775.603
6	1	60	700	50.26	831.773
7	0.75	30	700	45.84	1075.03
8	0.75	60	550	49.98	1046.89
9	0.75	90	400	54.58	687.452
10	0.75	90	700	42.34	941.61
11	0.75	30	400	59.66	263.71
12	1	60	400	64.22	404.38
13	0.75	60	550	55.36	997.296
14	0.5	90	550	50.75	864.028
15	0.5	60	400	58.42	282.526
16	0.75	60	550	51	996.46
17	0.5	60	700	46.2	653.49

where q_e and q_t are adsorption capacity at equilibrium and at a time 't' min, respectively (mg/g). K_1 is the rate constant of pseudo first order (min^{-1}), and K_2 is the rate constant of pseudo second order (g/mg min)

3 Results and discussion

3.1 Proximate analysis

Prepared jackfruit peel powder (precursor) was utilized for the analysis of moisture content, volatile matter, ash content, and fixed carbon. As illustrated in Table 3, ash content being in the lower range makes the considered primal matter suitable for AC preparation as a lesser loss would occur during carbonization [28], and a higher amount of volatile matter is preferred as empty pores would be left behind after degradation of volatile matter, implying to the formation of porous adsorbent [29].

3.2 Thermogravimetric analysis

Prediction of the degradation behavior of jackfruit peel was performed by thermogravimetric analysis. TGA provides the primary data required for AC synthesis, as presented in Fig. 2. A remarkable degradation is visible between 200 and 350°C. Prior to this, the degradation is due to moisture content loss in jackfruit peel. Agro-waste is basically lignocellulosic biomass (cellulose, hemicellulose, and lignin). Degradation of hemicellulose and cellulose begins nearly from (200–260°C) and (240–300°C) respectively. Lignin is comparatively more thermostable

and has a higher range of degradation; 400°C is considered the initial range of carbonization as the minute degradation ahead of it can be ignored caused by some non-combustible biomaterial.

3.3 Regression modeling

RSM was executed using a three-factor two-level BBD where the effect of each of the parameters, along with their interaction effect, was inspected on multiple responses with the selected two levels, as mentioned in Table 1. The design of the experimental runs and the calculated yield and iodine value after the performance of each of the experimental runs are mentioned in Table 2. As per the experimentally obtained data, the quadratic model was considered to be the most appropriate model among the other models like linear, cubic, two-factor interaction, etc., by the software named Design Expert, version 13.0, as it exhibits lower standard deviation and higher R^2 value. The polynomial regression equation for the yield (Y_1) and iodine value (Y_2) is as follows:

$$Y_1 = + 52.03 + 3.24A - 2.95B - 6.53C - 3.98AB - 0.4350AC$$
$$+ 3950BC + 3.34A^2 - 0.8273B^2 - 0.5997C^2 \tag{9}$$

$$Y_2 = + 996.46 + 45.82A + 66.70B + 232.98C + 52.12AB$$
$$+ 14.11AC - 139.29BC - 161.71A^2 + 37.19B^2 - 291.70C^2 \tag{10}$$

Table 3 Proximate analysis of jackfruit peel

Sl. no.	Constituents	Amount (%)
1.	Moisture content	6
2.	Volatile matter	70.18
3.	Ash content	5.89
4.	Fixed carbon	17.93

The equations, as mentioned above, were used for the prediction of the responses. The + sign displays the beneficial influence of the term on the response, whereas the − sign displays the adverse impact of the term on the response. In Eq. 9 for yield, 52.03 is apparently independent of any individual factor or their interactions. The individual (A), 2nd order (A^2), and interaction (BC) terms have a positive impact on yield, whereas remaining terms, such as B, C, B^2, C^2, AB, and AC, have a negative influence on the yield of the synthesized carbon using chemical activator. From Eq. 10, it is evident that 996.46 is dependent on none of the terms of the quadratic model. All the linear order terms that are B, A, and C have a good influence on iodine value, 2nd-order term; B^2, along

with interactions AB and AC, also has a positive impact on iodine value, whereas 2nd-order terms A^2 and C^2 and interaction AC have an adverse effect on the iodine value.

3.4 Statistical analysis of variance

The statistical analysis of variance (ANOVA) of the BBD was analyzed in a software named Design Expert, version 13.0. It figures out whether the model is significant and fit or not. It also determines which of the terms (linear, quadratic, and interactions) are significant for the model. For which, the p value (probability value) should be <0.05 (confidence level of 95%) [30] for the model as well as the model terms. Tables 4 and 5 illustrate the model fittings for the responses Y_1 and Y_2, respectively.

With the p value of 0.0006 and F value of 17.06, the model is significant for yield% (Y_1), as visible in Table 4. In the ANOVA table for yield, the p value for B, A, C, AB, and A^2 is not more than 0.05, which is why these terms of the model are statistically significant. On the other hand, terms like B^2, C^2, the interaction between the IR and carbonization temperature (AC), and the interaction between activation time and carbonization temperature (BC) are statistically non-significant as the

Table 4 Analysis of variance (ANOVA) for the multilinear regression model of yield%

Source	Sum of squares	df	Mean square	F value	p value	
Model	609.24	9	67.69	17.06	0.0006	Significant
A-IR	83.92	1	83.92	21.14	0.0025	
B-Time	69.80	1	69.80	17.59	0.0041	
C-Temp	341.13	1	341.13	85.95	< 0.0001	
AB	63.28	1	63.28	15.94	0.0052	
AC	0.7569	1	0.7569	0.1907	0.6755	
BC	0.6241	1	0.6241	0.1572	0.7035	
A^2	47.05	1	47.05	11.85	0.0108	
B^2	2.88	1	2.88	0.7260	0.4224	
C^2	1.51	1	1.51	0.3816	0.5563	
Lack of fit	10.02	3	3.34	0.7526	0.5755	Not significant

Table 5 Analysis of variance (ANOVA) for the multilinear regression model of iodine no.

Source	Sum of squares	df	Mean square	F value	p value	
Model	1.067E + 06	9	1.186E + 05	41.54	< 0.0001	Significant
A-IR	16,797.76	1	16,797.76	5.88	0.0457	
B-Time	35,593.39	1	35,593.39	12.47	0.0096	
C-Temp	4.342E + 05	1	4.342E + 05	152.12	< 0.0001	
AB	10,867.96	1	10,867.96	3.81	0.0920	
AC	796.05	1	796.05	0.2789	0.6138	
BC	77,607.37	1	77,607.37	27.19	0.0012	
A^2	1.101E + 05	1	1.101E + 05	38.57	0.0004	
B^2	5824.63	1	5824.63	2.04	0.1962	
C^2	3.583E + 05	1	3.583E + 05	125.51	< 0.0001	
Lack of fit	16,022.14	3	5340.71	5.39	0.0686	Not significant

Table 6 Model validation

IR	Carbonization temperature	Activation time	Yield (%)		Iodine no. (mg/g)	
			Predicted	Actual	Predicted	Actual
0.74	603.08	89.15	46.16	54	1090.44	1163.3

p value is more than 0.05. The interaction of the impregnation ratio and activation time (AB) has the most significant influence on the yield of $ZnCl_2$-AC. The R^2 value of 0.9564 represents an inimitable degree of fit of the polynomial regression model. Only 0.0436 of the total variations cannot be justified by this model. The predicted R^2 of 0.7047 is in fair agreement with the value of 0.9003 of adjusted R^2, as the difference in-between them is not more than 0.2, portraying a decent predictableness of the model. The standard deviation is 1.99, which gives an overview of similarities between the actual and predicted values for yield (Y_1). Coeff. of variation (CV) is 3.76, which shows good precision of the model. The CV below the value of 10% makes the model highly reliable [31]. The adequate precision is a value that represents the signal-to-noise ratio, and its value is greater than 4, which is desirable. The p value of the lack of fit of 0.5755 (insignificant) is preferable.

In Table 5 of ANOVA for iodine value, the model is significant with a probability value less than 0.0001 and F value of 41.54. All the terms of linear type (A, B, and C), terms of 2nd order type like A^2, C^2, and interaction of activation time and temperature (BC) are statistically significant. All the other terms are non-significant. The R^2 value of 0.9816 depicts that there is only 0.0184 of the total data that the current prescribed model cannot explain The difference between adjusted R^2 and predicted R^2 is within 0.2, which displays good model predictability. The CV of 6.67% confirmed the experimental accuracy. Models with higher F value and p value < 0.001 exhibit that the responses are well explained by their respective model equations [32].

The graphical representation of the actual data Vs predicted data for both the responses yield (Y_1) and iodine value (Y_2) is displayed in Fig. 3a, b. The predicted values are the data obtained by the model, and the actual data is the experimental data.

From the figures of actual data vs predicted data for yield and iodine value, it has been analyzed that as the data points are dispersed adjacent to the diagonal line, the correlation between the experimental data and the predicted data is proper [33]. It also implies to a good correlation of independent variables with the responses.

3.5 Interaction effect of process parameters on the responses

In Design Expert Software version 13.0, 3-dimensional graphs were produced for each model response (yield and iodine value) using the significant interactions of the process parameters. Two parameters vary between the levels, and the third parameter is kept constant.

Figure 4, the 3-D plot of the simultaneous effect of IR and activation time on the yield, illustrates that with the increase in the impregnation ratio, the yield increases, which can be due to polymerization due to the reaction between the activating agent and the biomass. With the increase in time, the yield decreases due to the degradation of the volatile substances caused by the reaction between activating agent and biomass.

Figure 5 represents the interaction between carbonization temperature and activation time and their impact on the iodine value. Initially, time and temperature trigger iodine value to increase, caused by the degradation of volatile matter with the prolonged intensification of reaction leading to pore formations. But beyond a certain temperature, the pore structure starts to break due to less endurance, causing a reduction in the volume of the pores along with the specific surface area of the carbon. Das et al. [11] also reported that temperature handles the rate at which the reaction occurs, whereas time handles the extent of the reaction required to develop a well-formed pore structure. Liu et al. [34] also explained similar results illustrating the increase and decrease in iodine value. The increasing iodine value is due to the uniformity in the formation of the micropores because of the reaction between carbon and water. Further rise in temperature expanded the micropores to mesopores or macropores, which caused the reduction in iodine value. Simultaneously, prolonged time caused burnoff of the pores resulting in less iodine value.

3.6 Parameter optimization

For optimization of AC synthesis, a maximum iodine value and a moderate to high yield were preferred. The iodine value specifies the effectiveness of the material, and yield directly influences the price of the activated carbon. Numerical optimization was done to get the best probable optimized value for the responses. The yield was set to be 'in range,' and the iodine value was set to be 'maximum.' The estimation of the optimum values for the independent variables is IR, A = 0.74; time, B = 89.15 min; and temperature, C = 603°C to attain a yield of 46.16% and iodine value of 1090.44 mg/g, which is presented in Fig. 6. It was verified by experimenting with the predicted independent variables.

An iodine value of 1163.3 mg/g and a yield of 54% were acquired as experimental results. The experimented data values were close to that of the estimations obtained from the model, as displayed in Table 6. Thus, RSM-BBD has displayed to be an excellent fit for current experimental data.

3.7 Characterization of precursor and optimized ZnCl$_2$-AC

3.7.1 Scanning electron microscope (SEM) and energy dispersive X-ray (EDX)

The surface morphology of JPP and prepared AC by zinc chloride activation (ZnCl$_2$-AC) was analyzed by scanning electron microscopy (SEM), imaging at 500× magnification as displayed in Fig. 7. It clearly demonstrated a very rough, irregular surface, and broken at some part of the surface. The ZnCl$_2$-AC showed the presence of a porous surface, and it was full of cavities of heterogeneous shapes and sizes, which were the opening ends of channel-like pores [35]. The cavities were the result of the evaporation of zinc chloride during the process of activation and leaving behind the pore cavities [36]. The release of the most volatile organic material resulted in the formation of pores on the surface [37].

The energy dispersive X-ray analysis (EDX) was performed to acquire the proportionate composition of the elements in JPP and ZnCl$_2$-AC. Carbon and oxygen were the major components observed in AC, with some traces of potassium, zinc, and chlorine. Both JPP and ZnCl$_2$-AC have a peak at approximately 2 keV, which is because the gold coating on the surface of both samples makes them conductive [38].

3.7.2 Fourier transform infrared spectroscopy (FTIR)

The FTIR analysis was done to identify the functional group of the raw sample (JPP) and the ZnCl$_2$-AC sample, as presented in Fig. 8. The broad peak around 3392 cm^{-1} and 3406 cm^{-1} is identified as the O–H stretch (hydroxyl group) or –NH$_2$ (amines group) [39, 40]. The sharp peak at 2920 cm^{-1}, 2922 cm^{-1}, 2850 cm^{-1}, and 2851 cm^{-1} is associated with C–H aromatic and C–H aliphatic stretching vibrations [41]. The peak of 1736 cm^{-1} is attributed to the presence of the C=O stretch of the aldehyde group [42]. The peaks at 1594 cm^{-1} and 1612 cm^{-1} show the presence of the C=O stretch (lactone group) [11] and C=C stretch [41, 43]. The 1453 cm^{-1} and 1404 cm^{-1} peaks may indicate the presence of C–H bend [42]. The peak at 1256 cm^{-1} indicates C–O stretch [43]. The peak at 1030 cm^{-1} and 1045 cm^{-1} indicates the C–O vibrations [44]. The region 1000 cm^{-1}–1280 cm^{-1} indicates the presence of ether group (C–O–C) [45]. The region less than 1000 cm^{-1} is called the fingerprint region. It is a complex region and quite difficult to identify the functional groups. The weaker peaks from 670 to 900 cm^{-1} can be due to C–H vibrations on the aromatic rings; 610 cm^{-1}–680 cm^{-1} peaks indicate the presence of C–H (alkyne groups) [11].

The FTIR spectra show a reduction of peaks in the AC compared to the raw sample as it occurs due to less absorbance in the region from 2800 to 3500 cm^{-1} due to the loss of hydroxyl groups. This is because of the carbonization of the JPP and activation using ZnCl$_2$, which acts as a dehydrating agent and breaks some bonds accompanied by heat [11]. The reduction in the intensity of the peaks in 1000 cm^{-1}–1200 cm^{-1} might have been caused by the oxygen reduction after activation [45]. Decreasing some of the bands and disappearance of certain peaks in the region of 1000 cm^{-1}–2000 cm^{-1} are also related to the degradation of the lignocellulosic matter after chemical treatment of the raw sample [46].

3.7.3 X-ray diffraction (XRD)

Evaluation of certain properties of JPP and ZnCl$_2$-AC was done by X-ray diffraction (XRD), presented in Fig. 9. As seen from the pattern of the raw sample, a significant peak appeared around $2\theta = 25.53°$ indicated the presence of organized crystalline cellulose material [47]. After activation and carbonization, there is a little shift in the peak which may depict the degradation of the lignocellulosic matter. The broad peak between $2\theta = 15°$ and 35° in the ZnCl$_2$-AC reveals the amorphous phase of the AC. The presence of peaks around $2\theta = 26°$ and 29° exhibits the SiO$_2$ and CaCO$_3$ impurities, respectively [48]. Around $2\theta = 44°$, the peak depicts the presence of hexagonal graphite structure [49, 50]. The diffractogram showed sharp peaks due to the presence of various phases of zinc compounds such as ZnO, Zn(OH)$_2$, and many more [4, 51]. The sharp peak around $2\theta = 14°$ confirms the presence of SiO$_2$ impurity in jackfruit peel [47].

3.8 Comparison of yield and iodine value with other precursors

There have been many studies done on the preparation of AC using multiple activating agents. A comparison study has been done of the iodine value and percentage of yield with other AC synthesized from other agricultural waste precursors and activating agents. It has been illustrated in Table 7 that the obtained yield and iodine adsorption value of the ZnCl$_2$-AC have better results than many others.

3.9 Evaluation of adsorption properties of ZnCl$_2$-AC against industrial dye

The adsorption study was performed on an industrial dye called Remazol golden yellow (RGY), using the optimized

Table 7 Comparison of yield and iodine value of many ACs

Precursor	Chemical activator	Yield (%)	Iodine value (mg/g)	References
Barley husks	$ZnCl_2$	49.46%	907.88 mg/g	Cancino et.al [8]
Limonia-acidissima shell	H_3PO_4	42.6324%	951.889 mg/g	Das and Mishra [11]
Date palm bark wastes	H_3PO_4	52%	983 mg/g	Haghbin et al. [10]
Date stones	$ZnCl_2$	-	928.5 mg/g	Abderrahim et al. [9]
Coconut shells	H_3PO_4	47.5%	698.37 mg/g	Liang et al. [6]
Jackfruit peel	$ZnCl_2$	54%	1163.3 mg/g	Current work

Table 8 Isotherm parameters for RGY removal using AC

Model	Parameters	Value
Langmuir	q_m (mg/g)	14.679
	K_L (L/mg)	0.23
	R^2	0.977
Freundlich	K_F	3.166
	$1/n$	0.473
	R^2	0.991

Table 9 Kinetics parameter for the adsorption of RGY using AC

Model	Parameter	Value
Pseudo first order	K_1 (min^{-1})	0.0482
	$q_{e, \exp}$ (mg/g)	8.57
	q_e (mg/g)	0.1265
	R^2	0.8741
Pseudo second order	K_2 (g/mg min)	0.8032
	$q_{e,\exp}$ (mg/g)	8.57
	q_e (mg/g)	8.5837
	R^2	0.9998

activated carbon ($ZnCl_2$-AC) as an adsorbent. The impact of pH, contact period, amount of adsorbent, and initial concentration of RGY solution was studied systematically to check the adsorption capability of $ZnCl_2$-AC. RGY adsorption as a function of all the parameters mentioned above is illustrated in Fig. 10.

3.9.1 Effect of pH

Removal efficiency reduced from 97.78 to 92.94% as the pH went from 2 to 10, as depicted in Fig. 10a. The adsorption capacity also remains high for pH 2–10, as displayed in Fig. 11a. The removal efficiency is high irrespective of the pH of the solution. The decrease in the sorption was only 4.84% when pH increased from 2 to 10. The amphoteric behavior of the activated carbon is exhibited [52]. It can behave as a positive (+ ve) surface or negative (−ve) surface, depending upon the pH of the working solution. In acidic pH, the surface attains a positive charge. Electrostatic attraction of the colored anion of RGY dye happens towards the + ve surface of the adsorbent present in the solution[53]. In basic pH the $ZnCl_2$-AC surface possibly contains certain functional groups that attract the anionic dye particles. Electrostatic repulsion could have been less between the RGY dye ion and the −ve surface of $ZnCl_2$-AC.

3.9.2 Effect of adsorbent dosage

The adsorbent dosage effect was studied for a range of 0.05 to 0.5g of $ZnCl_2$-AC (pH: 6, contact period: 40 min, and initial RGY concentration: 50 mg/L). As per Fig. 10b, RGY adsorption subsequently increases from 85.95 to 96.69% with an increase in $ZnCl_2$-AC dosage from 0.05 to 0.2g,

Fig. 3 Plot of predicted response vs actual response for (**a**) yield and (**b**) iodine no.
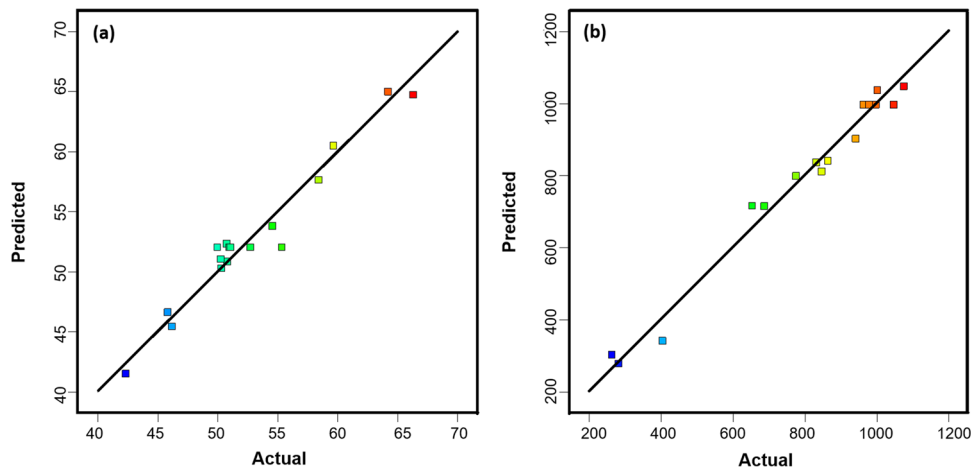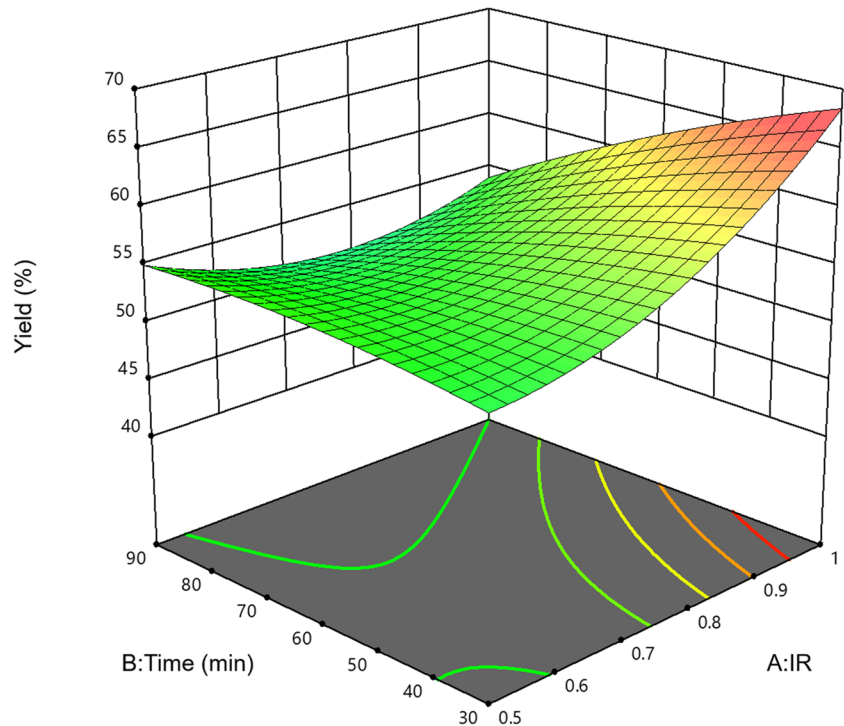
Fig. 4 Effect of activation time
and impregnation ratio and on
yield percentage

which substantiate the abundance of the active sites initially. However, the adsorption rises by only 2% on an additional increase of 0.1g $ZnCl_2$-AC, and for further increase in adsorbent, the removal efficiency remains almost constant. As mentioned by Liao et al. [54], spectrums of binding energy are all over the adsorbent surface on the active

sites. Adsorption is faster as the sites are exposed entirely for adsorption at a lower adsorbent dose and showing high q_e value (Fig. 11b), but at a higher dosage, the availability of higher sites decreases with a larger fraction of lower energy sites occupied, resulting in a lower q_e value. Active sites increase with the addition of the adsorbent amount in a

Fig. 5 Interaction effect of
carbonization temperature and
activation time on iodine no.
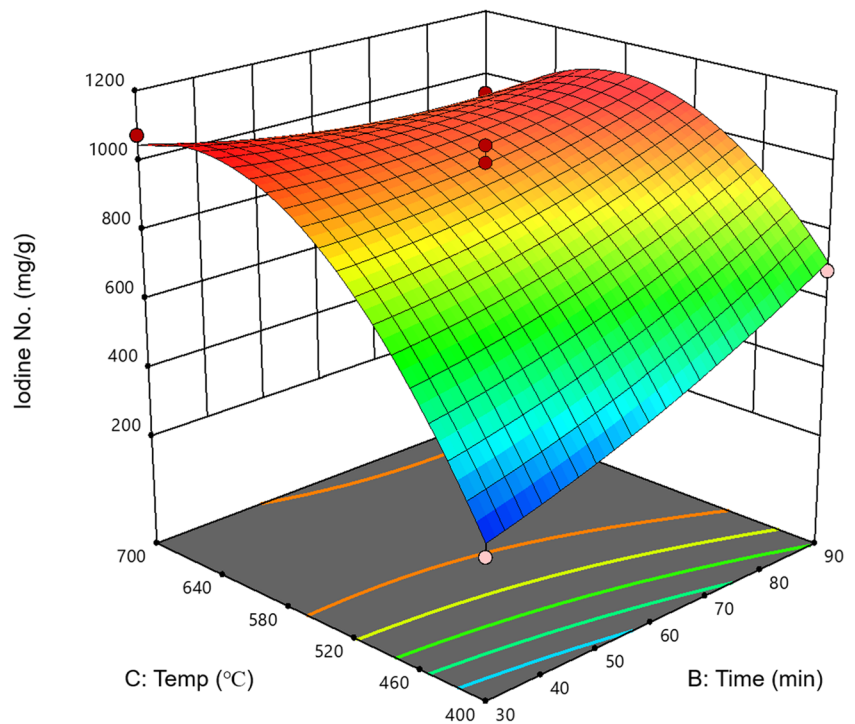
Fig. 6 Desirability approach
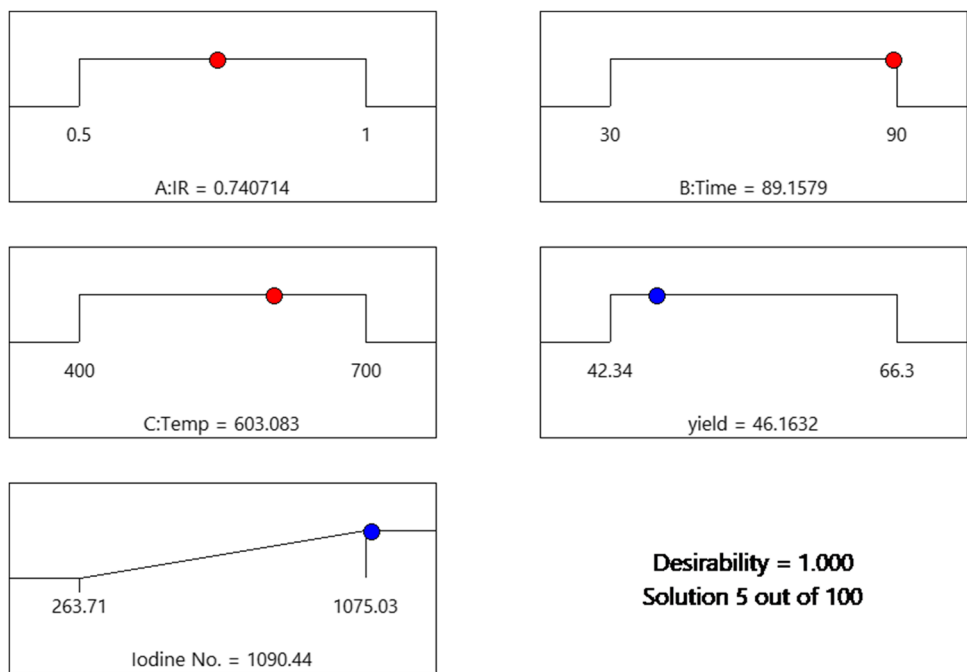
certain volume of working solution, but simultaneously there would be a drop in adsorption capacity as the sites remain unsaturated as dosage increases [55].

3.9.3 Effect of contact period

It is witnessed from the graph (Fig. 10c) that the RGY dye adsorption on $ZnCl_2$-AC is quite fast initially, where 90%

of the adsorption takes place at initial 5 min, and equilibrium is attained within 40 min. It can be interpreted that the whole vacant surface sites are initially available for adsorption, which gradually decreases, and after equilibrium, due to the repulsive force between the molecules at the sites, it is difficult to occupy the remaining vacant sites. It can also be understood that the active sites get blocked by the RGY molecules, leading to the fall in the adsorption rate

Fig. 7 **a**) SEM image of precursor (jackfruit peel). **b**) SEM image of optimized $ZnCl_2$-AC. **c**) EDX of precursor. **d**) EDX of optimized $ZnCl_2$-AC
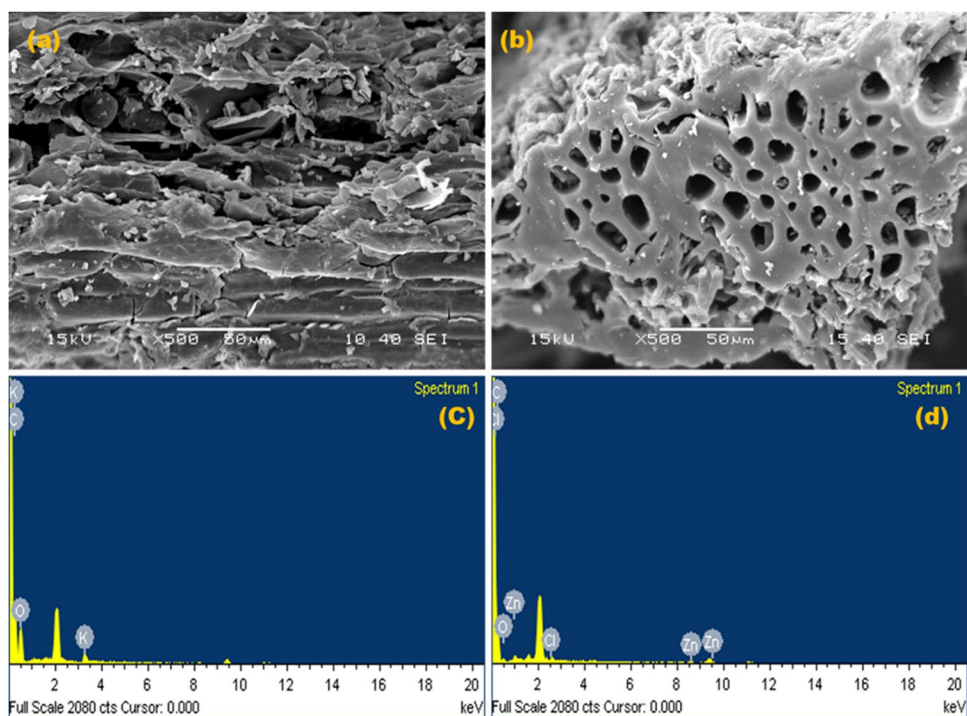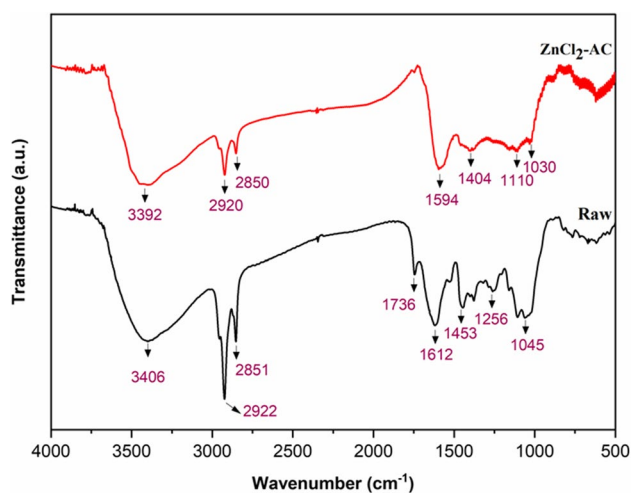
Fig. 8 FTIR spectra of JPP and ZnCl$_2$-AC

and causing dynamic equilibrium, after which there would be no substantial increase in RGY molecule adsorption on the ZnCl$_2$-AC surface [56].

3.9.4 Effect of initial RGY concentration

The impact was studied by varying the concentration of RGY from 10 to 100 mg/L. An increase in RGY concentration causes the removal efficiency to decrease while the adsorption capacity increases. It is reasonable, as adsorbents have a fixed amount of active sites accommodating only a certain concentration of the adsorbate. In the adsorption process' initial stage, more active sites are easily accessible. It facilitates the RGY dye molecules to get aggregated on the ZnCl$_2$-AC surface due to the driving force that surmounts the resistance among the interface of solid-solution. The
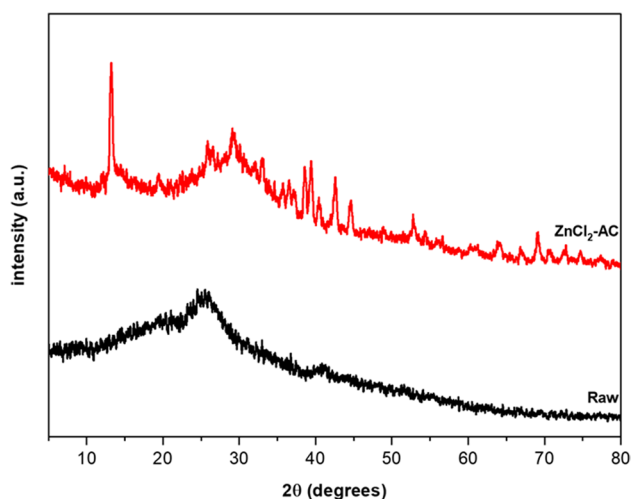
Fig. 9 XRD interpretation of raw sample (JPP) and ZnCl$_2$-AC

adsorption capacity hiked from 1.618 to 12.87 mg/g, as illustrated in Fig. 11d, apparently caused by the amplification of the driving force. On the contrary, the uptake efficiency falls from 97.1 to 77.2% (Fig. 10d) as the RGY dye molecules saturated the ZnCl$_2$-AC adsorption active sites [25, 56].

After studying the impact of all the affecting parameters on the adsorption of Remazol golden yellow dye from an aqueous solution, as mentioned above, the maximum removal efficiency was found to be nearly 97% for the optimum conditions as followed; 40 min of the contact period, 0.3 g of ZnCl$_2$-AC dose, and 10 mg/L of RGY solution at 6 pH.

3.10 Adsorption isotherm

The fundamental data acquired by the isotherms contributes to the knowledge of the unit operation of the adsorption at equilibrium [12, 14]. Experimentation includes the effect of various concentrations of RGY dye at 35°C after 40 min. Graphs are presented in Fig. 12. Evaluation of the adsorption data was tested by the Langmuir and Freundlich model by linear regression, as presented in Table 8. Among the two models with a higher coefficient of correlation of 0.991, Freundlich was depicted to be the best fit for the experimental data. Based on the assumptions of the Freundlich isotherm model, multilayer adsorption of Remazol golden yellow molecule occurs on energetically heterogeneous surface with sites having different affinity for adsorption. 1/n value of 0.473 (<1) implies favorability. Suhaimi et al. [5] acquired similar results as they utilized pomegranate peel mixed with carrot juice pulp which was activated using zinc chloride to remove crystal violet dye. Husein et al. [57] also showed the Freundlich model as the best-fitted isotherm while investigating H$_3$PO$_4$-activated algae-based activated carbon for methyl orange treatment.

3.11 Adsorption kinetics

Adsorption kinetics' information data accords with the mechanism pathway and residence time. The analysis was done in between two models, pseudo first and pseudo second order, in their linear form as presented in Fig. 13. As per the kinetic parameters presented in Table 9, the pseudo-second-order model better represents the experimental data with the coefficient of correlation closer to unity (0.9998) as compared to pseudo first order (R^2 = 0.8741). As per the assumptions related to pseudo second order, chemi-sorption is the reason for the removal process. The RGY dye ions are getting attached to the ZnCl$_2$-AC through chemical bonds. At the optimum condition of concentration of RGY dye solution, the inter-particle collision is less, which helps in faster bonding of

Fig. 10 Percentage removal data as per (**a**) pH, (**b**) adsorbent dose, (**c**) contact period, and (**d**) initial concentration
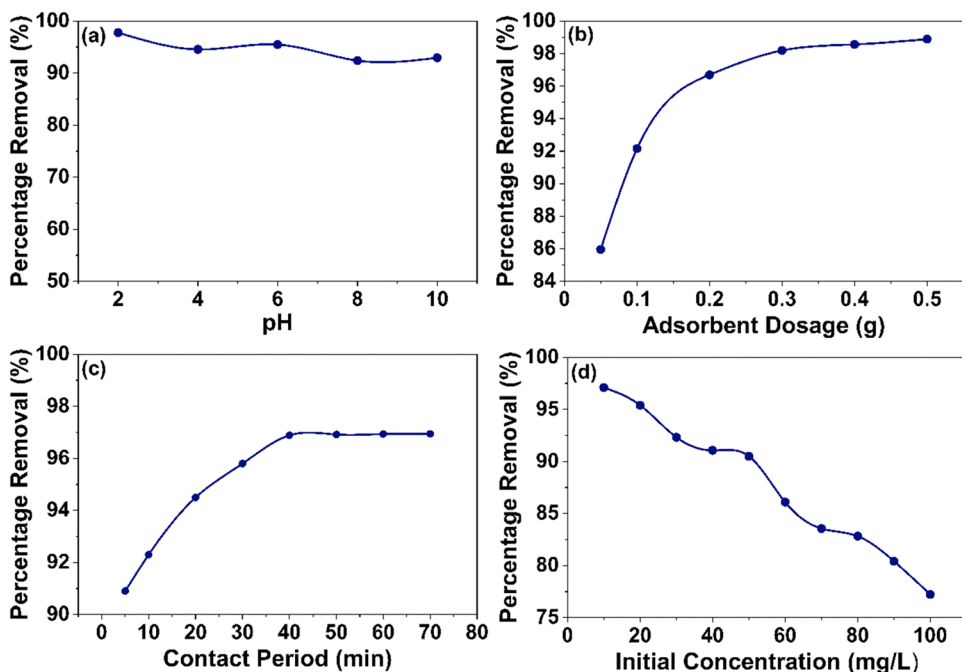
the adsorbate on the active sites of the ZnCl$_2$-AC surface. These results are parallel to the kinetic models investigated by Quimada et al. [16] while investigating the treatment of Erichrome black T using residual coffee grounds. As per the study executed by Raj et al. [58], Remazol brilliant blue R dye was adsorbed from an aqueous solution by utilizing sewage sludge biochar.

3.12 Adsorption mechanism of RGY dye

Many processes can possibly govern the adsorption route for RGY dye on ZnCl$_2$-AC. For example, pore diffusion, electrostatic interaction, π–π interaction, hydrogen bonding etc. [5]. Figure 14 demonstrates the possible interactions contributing to RGY dye adsorption onto ZnCl$_2$-AC. Pore diffusion is predominantly responsible for adsorption. Activated

Fig. 11 Effect of (**a**) pH, (**b**) adsorbent dosage, (**c**) contact period, and (**d**) initial concentration on adsorption capacity
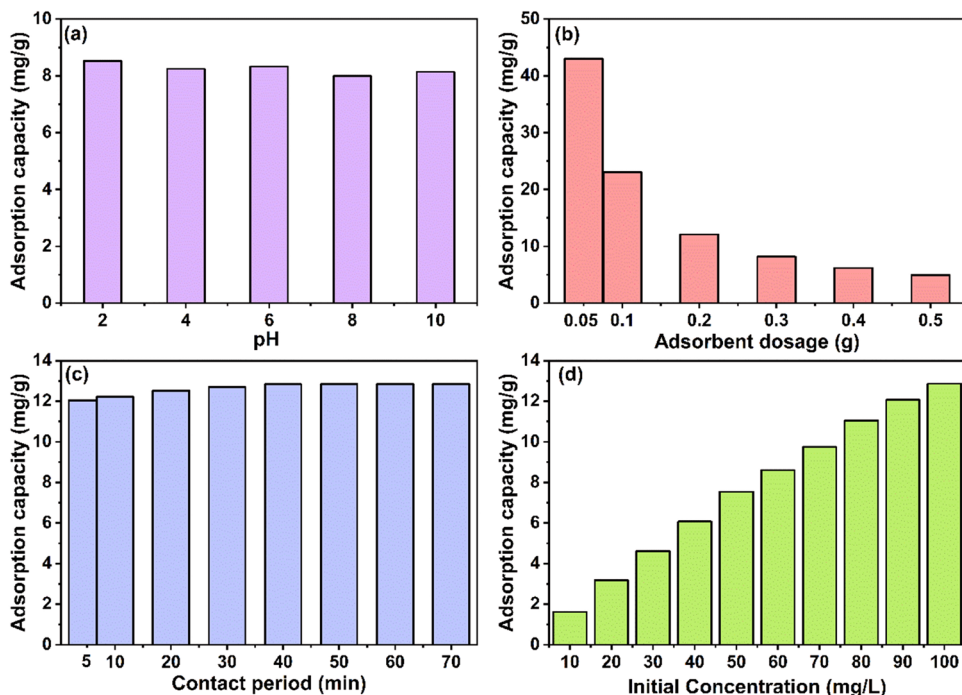
Fig. 12 (**a**) Langmuir isotherm model and (**b**) Fruendlich isotherm model for RGY adsorption on $ZnCl_2$-AC
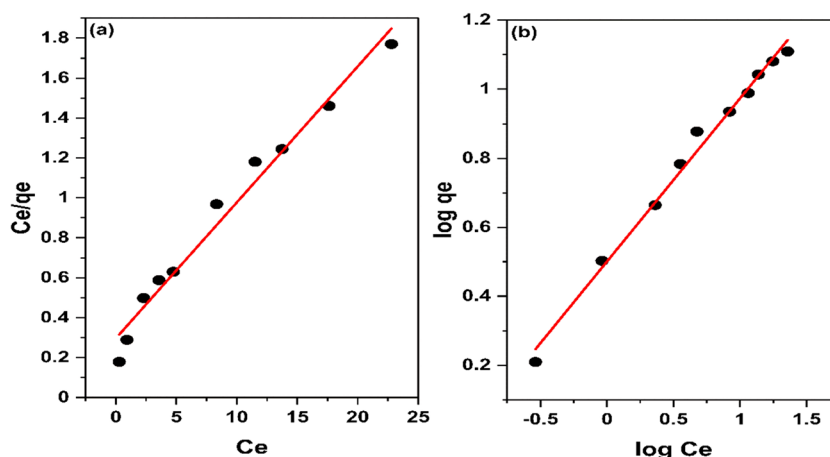
carbon ($ZnCl_2$-AC) combines macropores, mesopores, and micropores. RGY dye's molecular size is approximately 2 nm. RGY molecule entry is unhindered through macropores. Diffusion is relatively easy through mesopores. It could even pass through partial numbers of micropores, but it is very difficult to get through for some of the micropores. FTIR analysis provided the data illustrating the presence of O–H group and C=O group on the adsorbent's surface. RGY molecules with H acceptor oxygen atom are bonded with the hydroxyl group of $ZnCl_2$-AC by hydrogen bond. π-electron of the $ZnCl_2$-AC and π-electron of the benzene ring of the RGY molecule (electron donor and electron acceptor, respectively) are bonded with π–π interaction [59]. O^- group of $ZnCl_2$-AC engages with the benzene ring of the RGY molecule in n–π interaction.

3.13 Reusability of $ZnCl_2$-AC as adsorbent

The reusability of any synthesized adsorbent displays its stronghold in its valorization [60]. To test the reusability of

$ZnCl_2$-AC, distilled water, strong acid, and strong base were used to treat the adsorbent after each adsorption cycle. As displayed by the graph (Fig. 15), the RGY removal efficiency of $ZnCl_2$-AC decreases more after each cycle when desorbed with distilled water than hydrochloric acid. Treatment with sodium hydroxide exhibits consistent adsorption efficiency of more than 90% even after its 4th cycle. $ZnCl_2$-AC has the potential to be used at least 5 times.

4 Conclusion

An investigation had been carried out where activated carbon was synthesized using abundantly available agricultural waste jackfruit peel and activated using $ZnCl_2$. The optimization was practiced using the Box-Behnken design method with parameters: impregnation ratio, activation time, and carbonization temperature for the maximization of iodine value and yield. ANOVA was performed on quadratic models for each response to gain better relation among

Fig. 13 (**a**) Pseudo-first-order model and (**b**) pseudo-second-order model for RGY adsorption on $ZnCl_2$-AC
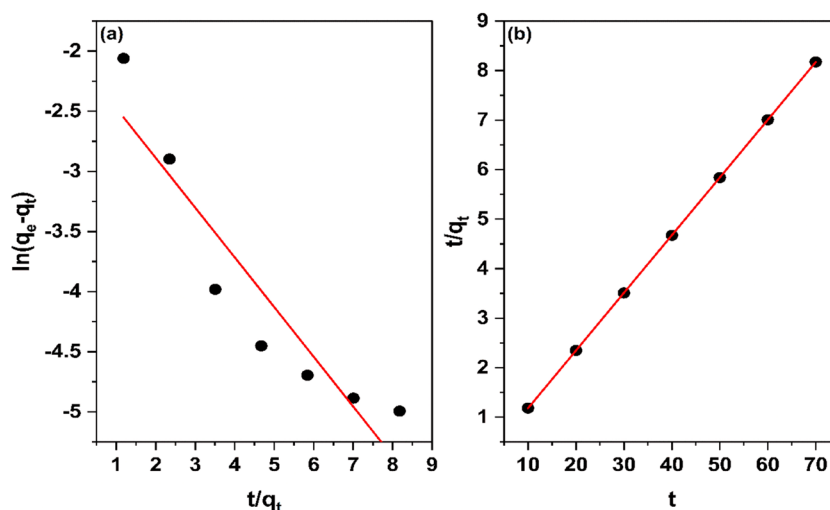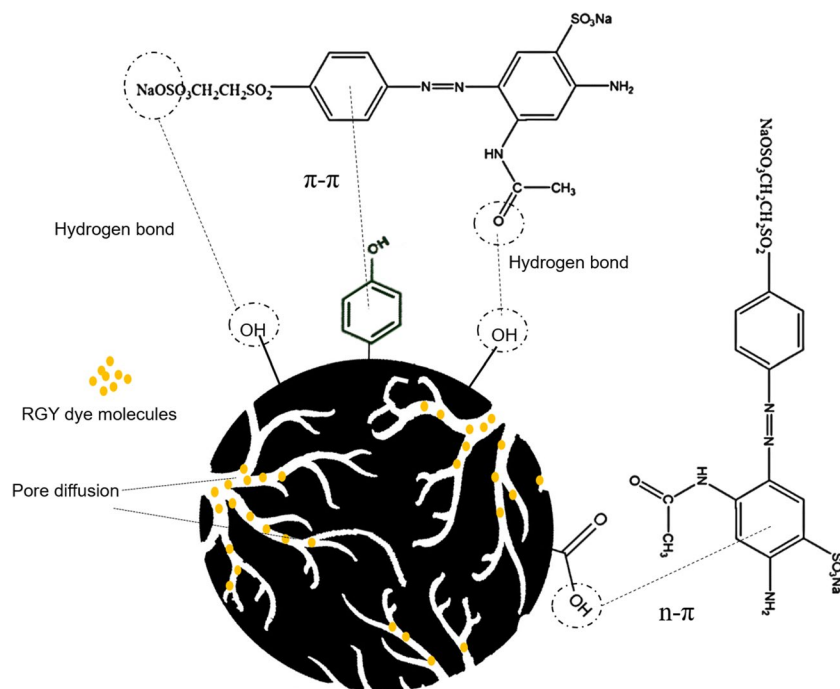
Fig. 14 Possible mechanism interaction of RGY adsorption on ZnCl$_2$-AC

the three variables, and a higher value of coefficient of correlation depicted a good fit of the model. Simultaneous optimization was engaged for the desirability approach for the optimum yield and iodine value conditions. For the current work, the maximum yield obtained was 46.16%, and the maximum iodine value obtained was 1090.44 mg/g for optimum conditions of 0.74 IR, 603.08°C carbonization temperature, and 89 min of activation time. This prediction of the model was validated by running an experiment that came to be almost similar to the predicted values. The response data was well compared with the literature data

showing high iodine adsorption value and yield. The SEM results depicted well-developed pore structures, and FTIR analysis assessed the presence of various functional groups. The adsorption performance displayed inimitable results when the optimized activated carbon was used as an adsorbent, with a high removal efficiency of 97% for an anionic dye (Remazol golden yellow). Freundlich isotherm model and pseudo-second-order model exhibited better representation of the experimental data. Pore diffusion, electrostatic interaction, π–π interaction, and hydrogen bonding were the cause of possible interactions. Multiple use is possible for up to 5th cycle. To sum up everything that has been stated so far, the above results support the use of locally available precursor, making it economical to prepare chemically activated carbon in an efficient manner with more control over the desired results.

Author contribution Experimentation, data analysis, and manuscript preparation are done by PM, and conceptualization, editing, and supervision are done by SM.

Declarations

Fig. 15 Reusability test of ZnCl$_2$-AC

References

1. Adejumo IO, Adebiyi OA (2020) Agricultural solid wastes: causes, effects, and effective management. In: Strategies of sustainable solid waste management. IntechOpen, London, UK

2. Koul B, Yakoob M, Shah MP (2022) Agricultural waste management strategies for environmental sustainability. Environ Res 206:112285

3. Modesto HR, Lemos SG, dos Santos MS et al (2021) Activated carbon production from industrial yeast residue to boost up circular bioeconomy. Environ Sci Pollut Res 28:24694–24705. https://doi.org/10.1007/s11356-020-10458-z

4. Simões dos Reis G, Bergna D, Tuomikoski S et al (2022) Preparation and characterization of pulp and paper mill sludge-activated biochars using alkaline activation: a Box–Behnken design approach. ACS Omega 7:32620–32630. https://doi.org/10.1021/acsomega.2c04290

5. Suhaimi A, Abdulhameed AS, Jawad AH et al (2022) Production of large surface area activated carbon from a mixture of carrot juice pulp and pomegranate peel using microwave radiation-assisted ZnCl2 activation: an optimized removal process and tailored adsorption mechanism of crystal violet dye. Diam Relat Mater 130:109456. https://doi.org/10.1016/j.diamond.2022.109456

6. Liang Q, Liu Y, Chen M et al (2020) Optimized preparation of activated carbon from coconut shell and municipal sludge. Mater Chem Phys 241:122327. https://doi.org/10.1016/j.matchemphys.2019.122327

7. Mozhiarasi V, Natarajan TS (2022) Bael fruit shell–derived activated carbon adsorbent: effect of surface charge of activated carbon and type of pollutants for improved adsorption capacity. Biomass Convers Biorefinery. https://doi.org/10.1007/s13399-022-03211-8

8. Loredo-Cancino M, Soto-Regalado E, Cerino-Córdova FJ et al (2013) Determining optimal conditions to produce activated carbon from barley husks using single or dual optimization. J Environ Manag 125:117–125. https://doi.org/10.1016/j.jenvman.2013.03.028

9. Abderrahim N, Boumnijel I, Ben AH, Djellabi R (2022) Heat and ZnCl2 chemical carbonization of date stone as an adsorbent: optimization of material fabrication parameters and adsorption studies. Environ Sci Pollut Res 29:46038–46048. https://doi.org/10.1007/s11356-022-19132-y

10. Haghbin MR, Niknam Shahrak M (2021) Process conditions optimization for the fabrication of highly porous activated carbon from date palm bark wastes for removing pollutants from water. Powder Technol 377:890–899. https://doi.org/10.1016/j.powtec.2020.09.051

11. Das S, Mishra S (2017) Box-Behnken statistical design to optimize preparation of activated carbon from Limonia acidissima shell with desirability approach. J Environ Chem Eng 5:588–600. https://doi.org/10.1016/j.jece.2016.12.034

12. Özsin G, Kılıç M, Apaydın-Varol E, Pütün AE (2019) Chemically activated carbon production from agricultural waste of chickpea and its application for heavy metal adsorption: equilibrium, kinetic, and thermodynamic studies. Appl Water Sci 9:56. https://doi.org/10.1007/s13201-019-0942-8

13. Genli N, Kutluay S, Baytar O, Şahin Ö (2022) Preparation and characterization of activated carbon from hydrochar by hydrothermal carbonization of chickpea stem: an application in methylene blue removal by RSM optimization. Int J Phytoremediation 24:88–100. https://doi.org/10.1080/15226514.2021.1926911

14. Rai MK, Shahi G, Meena V et al (2016) Removal of hexavalent chromium Cr (VI) using activated carbon prepared from mango kernel activated with H3PO4. Resource-Efficient Technologies 2:S63–S70. https://doi.org/10.1016/j.reffit.2016.11.011

15. Mashhadi S, Sohrabi R, Javadian H et al (2016) Rapid removal of Hg (II) from aqueous solution by rice straw activated carbon prepared by microwave-assisted H2SO4 activation: kinetic, isotherm and thermodynamic studies. J Mol Liq 215:144–153. https://doi.org/10.1016/j.molliq.2015.12.040

16. Quimada NE, Sioson AS, Sutopo F, Mabayo VIF (2023) Response surface optimization of the efficiency of ZnCl2-impregnated activated carbon from residual coffee grounds in the removal of Eriochrome Black T dye-contaminated wastewater. Biomass Convers Biorefinery. https://doi.org/10.1007/s13399-023-04090-3

17. Liew RK, Azwar E, Yek PNY et al (2018) Microwave pyrolysis with KOH/NaOH mixture activation: a new approach to produce micro-mesoporous activated carbon for textile dye adsorption. Bioresour Technol 266:1–10. https://doi.org/10.1016/j.biortech.2018.06.051

18. Pimentel CH, Freire MS, Gómez-Díaz D, González-Álvarez J (2023) Preparation of activated carbon from pine (Pinus radiata) sawdust by chemical activation with zinc chloride for wood dye adsorption. Biomass Convers Biorefinery. https://doi.org/10.1007/s13399-023-04138-4

19. Astuti W, Sulistyaningsih T, Prastiyanto D et al (2023) Influence of lignocellulosic composition in biomass waste on the microstructure and dye adsorption characteristics of microwave-assisted ZnCl2 activated carbon. Biomass Convers Biorefinery. https://doi.org/10.1007/s13399-023-04281-y

20. Maity S, Bajirao Patil P, SenSharma S, Sarkar A (2022) Bioremediation of heavy metals from the aqueous environment using Artocarpus heterophyllus (jackfruit) seed as a novel biosorbent. Chemosphere 307:136115. https://doi.org/10.1016/j.chemosphere.2022.136115

21. Kalse SB, Swami SB (2022) Recent application of jackfruit waste in food and material engineering: a review. Food Biosci 48:101740. https://doi.org/10.1016/j.fbio.2022.101740

22. Mohamad Yusop MF, Abdullah AZ, Ahmad MA (2023) Malachite green dye adsorption by jackfruit based activated carbon: optimization, mass transfer simulation and surface area prediction. Diam Relat Mater 136:109991. https://doi.org/10.1016/j.diamond.2023.109991

23. Awitdrus A, Yusra DA, Taer E et al (2022) Biomass conversion into activated carbon as a sustainable energy material for the development of supercapacitor devices. Energy Sources A: Recovery Util Environ Eff 44:3349–3359. https://doi.org/10.1080/15567036.2022.2064941

24. Magesh N, Renita AA, Siva R et al (2022) Adsorption behavior of fluoroquinolone(ciprofloxacin) using zinc oxide impregnated activated carbon prepared from jack fruit peel: kinetics and isotherm studies. Chemosphere 290:133227. https://doi.org/10.1016/j.chemosphere.2021.133227

25. Behloul H, Ferkous H, Bougdah N et al (2022) New insights on the adsorption of CI-Reactive Red 141 dye using activated carbon prepared from the ZnCl2-treated waste cotton fibers: statistical physics, DFT, COSMO-RS, and AIM studies. J Mol Liq 364:119956. https://doi.org/10.1016/j.molliq.2022.119956

26. Reddy KSK, Al Shoaibi A, Srinivasakannan C (2012) Activated carbon from date palm seed: process optimization using response surface methodology. Waste Biomass Valorization 3:149–156. https://doi.org/10.1007/s12649-011-9104-4

27. Wang J, Guo X (2020) Adsorption isotherm models: classification, physical meaning, application and solving method. Chemosphere 258:127279. https://doi.org/10.1016/j.chemosphere.2020.127279

28. Feng P, Li J, Wang H, Xu Z (2020) Biomass-based activated carbon and activators: preparation of activated carbon from corncob by chemical activation with biomass pyrolysis liquids. ACS Omega 5:24064–24072. https://doi.org/10.1021/acsomega.0c03494

29. Zhang J, Zhong Z, Shen D et al (2011) Preparation of bamboo-based activated carbon and its application in direct carbon fuel cells. Energy Fuel 25:2187–2193. https://doi.org/10.1021/ef200161c

30. Pinheiro DR, Neves RDF, Paz SPA (2021) A sequential Box-Behnken Design (BBD) and Response Surface Methodology (RSM) to optimize SAPO-34 synthesis from kaolin waste. Microporous Mesoporous Mater 323:111250. https://doi.org/10.1016/j.micromeso.2021.111250

31. Jawad AH, Sahu UK, Jani NA et al (2022) Magnetic crosslinked chitosan-tripolyphosphate/MgO/Fe3O4 nanocomposite for reactive blue 19 dye removal: optimization using desirability function approach. Surf Interfaces 28:101698. https://doi.org/10.1016/j.surfin.2021.101698

32. Senthilkumar T, Chattopadhyay SK, Miranda LR et al (2017) Optimization of activated carbon preparation from pomegranate peel (Punica granatum Peel) using RSM optimization of activated carbon preparation from pomegranate peel (Punica granatum peel) using RSM. Chem Eng Commun 204:238–248. https://doi.org/10.1080/00986445.2016.1262358

33. Jawad AH, Saud Abdulhameed A, Wilson LD et al (2021) High surface area and mesoporous activated carbon from KOH-activated dragon fruit peels for methylene blue dye adsorption: optimization and mechanism study. Chin J Chem Eng 32:281–290. https://doi.org/10.1016/j.cjche.2020.09.070

34. Liu C, Liang L, Han X et al (2022) Optimized preparation of activated carbon from furfural residue using response surface methodology and its application for bisphenol S adsorption. Water Sci Technol 85:811–826. https://doi.org/10.2166/wst.2021.634

35. Amin M, Chung E, Shah HH (2022) Effect of different activation agents for activated carbon preparation through characterization and life cycle assessment. Int J Environ Sci Technol. https://doi.org/10.1007/s13762-022-04472-6

36. Raut ER, Bedmohata MA, Chaudhari AR (2022) Comparative study of preparation and characterization of activated carbon obtained from sugarcane bagasse and rice husk by using H3PO4 and ZnCl2. Materials Today: Proceedings 66:1875–1884. https://doi.org/10.1016/j.matpr.2022.05.413

37. El-Nemr MA, El Nemr A, Hassaan MA et al (2022) Microporous activated carbon from Pisum sativum pods using various activation methods and tested for adsorption of acid orange 7 dye from water. Molecules 27:4840. https://doi.org/10.3390/molecules27154840

38. Kumar H, Patel M, Mohan D (2019) Simplified batch and fixed-bed design system for efficient and sustainable fluoride removal from water using slow pyrolyzed okra stem and black gram straw biochars. ACS Omega 4:19513–19525. https://doi.org/10.1021/acsomega.9b00877

39. Ravulapalli S, Ravindhranath K (2017) Defluoridation studies using active carbon derived from the barks of Ficus racemosa plant. J Fluor Chem 193:58–66. https://doi.org/10.1016/j.jfluchem.2016.11.013

40. Leonard J, Sivalingam S, Srinadh RV, Mishra S (2023) Efficient removal of hexavalent chromium ions from simulated wastewater by functionalized anion exchange resin: process optimization, isotherm and kinetic studies. Environ Chem Ecotoxicol 5:98–107. https://doi.org/10.1016/j.enceco.2023.03.001

41. Mustafa I, Fathurrahmi S, Farida M, Ahmad K (2022) Palm shell-derived activated carbon adsorbent is better than that of coconut shell: comparative studies of COD adsorption from palm oil mill effluent. Rasayan J Chem 15:738–744. https://doi.org/10.31788/RJC.2022.1526804

42. Jayashree DE, Kumar PS, Ngueagni PT et al (2021) Effective removal of excessive fluoride from aqueous environment using activated pods of Bauhinia variegata: batch and dynamic analysis. Environ Pollut 272:115969. https://doi.org/10.1016/j.envpol.2020.115969

43. Araga R, Soni S, Sharma CS (2017) Fluoride adsorption from aqueous solution using activated carbon obtained from KOH-treated jamun (Syzygium cumini) seed. J Environ Chem Eng 5:5608–5616. https://doi.org/10.1016/j.jece.2017.10.023

44. Sahu N, Singh J, Koduru JR (2021) Removal of arsenic from aqueous solution by novel iron and iron–zirconium modified activated carbon derived from chemical carbonization of Tectona grandis sawdust: isotherm, kinetic, thermodynamic and breakthrough curve modelling. Environ Res 200:111431. https://doi.org/10.1016/j.envres.2021.111431

45. Bai X, Quan B, Kang C et al (2022) Activated carbon from tea residue as efficient absorbents for environmental pollutant removal from wastewater. Biomass Convers Biorefinery. https://doi.org/10.1007/s13399-022-02316-4

46. Georgin J, Franco DSP, Netto MS, et al (2022) Effective adsorption of harmful herbicide diuron onto novel activated carbon from Hovenia dulcis. Colloids Surf A Physicochem Eng Asp 654:129900. https://doi.org/10.1016/j.colsurfa.2022.129900

47. Luo X, Cai Y, Liu L, Zeng J (2019) Cr(VI) adsorption performance and mechanism of an effective activated carbon prepared from bagasse with a one-step pyrolysis and ZnCl2 activation method. Cellulose 26:4921–4934. https://doi.org/10.1007/s10570-019-02418-9

48. Ma Y, Wang Q, Wang X et al (2015) A comprehensive study on activated carbon prepared from spent shiitake substrate via pyrolysis with ZnCl2. J Porous Mater 22:157–169. https://doi.org/10.1007/s10934-014-9882-8

49. Benmahdi F, Oulmi K, Khettaf S et al (2021) Synthesis and characterization of microporous granular activated carbon from Silver berry seeds using ZnCl 2 activation. Fuller Nanotub Carbon Nanostructures 29:657–669. https://doi.org/10.1080/1536383X.2021.1878154

50. Kumar A, Mohan Jena H (2015) High surface area microporous activated carbons prepared from Fox nut (Euryale ferox) shell by zinc chloride activation. Appl Surf Sci 356:753–761. https://doi.org/10.1016/j.apsusc.2015.08.074

51. Danish M, Ahmad T, Hashim R et al (2018) Comparison of surface properties of wood biomass activated carbons and their application against rhodamine B and methylene blue dye. Surf Interfaces 11:1–13. https://doi.org/10.1016/j.surfin.2018.02.001

52. Al-Degs Y (2000) Effect of carbon surface chemistry on the removal of reactive dyes from textile effluent. Water Res 34:927–935. https://doi.org/10.1016/S0043-1354(99)00200-6

53. Vijayaraghavan K, Won SW, Yun Y-S (2009) Treatment of complex Remazol dye effluent using sawdust- and coal-based activated carbons. J Hazard Mater 167:790–796. https://doi.org/10.1016/j.jhazmat.2009.01.055

54. Liao X, Shi B (2005) Adsorption of fluoride on zirconium(IV)-impregnated collagen fiber. Environ Sci Technol 39:4628–4632. https://doi.org/10.1021/es0479944

55. Ishak Z, Salim S, Kumar D (2021) Adsorption of methylene blue and reactive black 5 by activated carbon derived from tamarind seeds. Trop Aqua Soil Poll 2:1–12. https://doi.org/10.53623/tasp.v2i1.26

56. Patra T, Mohanty A, Singh L et al (2022) Effect of calcination temperature on morphology and phase transformation of MnO2 nanoparticles: a step towards green synthesis for reactive dye adsorption. Chemosphere 288:132472. https://doi.org/10.1016/j.chemosphere.2021.132472

57. Husien S, El-taweel RM, Mohamed N et al (2023) Potentials of algae-based activated carbon for the treatment of M.orange in wastewater. Case Studies in Chemical and Environmental. Engineering 7:100330. https://doi.org/10.1016/j.cscee.2023.100330

58. Raj A, Yadav A, Rawat AP et al (2021) Kinetic and thermodynamic investigations of sewage sludge biochar in removal of Remazol Brilliant Blue R dye from aqueous solution and evaluation of residual dyes cytotoxicity. Environ Technol Innov 23:101556. https://doi.org/10.1016/j.eti.2021.101556

59. Khasri A, Jamir MRM, Ahmad AA, Ahmad MA (2021) Adsorption of Remazol Brilliant Violet 5R dye from aqueous solution onto melunak and rubberwood sawdust based activated carbon: interaction mechanism, isotherm, kinetic and thermodynamic properties. Desalin Water Treat 216:401–411. https://doi.org/10.5004/dwt.2021.26852

60. Singh J, Kumar A, Pathak A, Palai T (2023) Adsorptive removal of arsenic(III) from contaminated water using rice husk, tea waste and sugarcane bagasse bio-adsorbents. Water Air Soil Pollut 234:308. https://doi.org/10.1007/s11270-023-06308-6